Structure and Ferroelectric Behaviour of $Na_{0.5}Bi_{0.5}TiO_3$-$KNbO_3$ Ceramics

G. Wang[1], D.A. Hall[1], T.P Comyn[2], L. Daniel[3] and A.K. Kleppe[4]

[1]School of Materials, University of Manchester, Manchester, M13 9PL, UK.
[2]Institute for Materials Research, University of Leeds, LS2 9JT, UK.
[3]GeePs (CNRS UMR8507, CentraleSupelec, UPMC, Univ Paris-Sud), 91192 Gif Sur Yvette cedex, France.
[4]Diamond Light Source Ltd, Diamond House, Harwell Science and Innovation Campus, Didcot, Oxfordshire, OX11 0DE, UK.

Abstract

Lead-free piezoelectric ceramics, (1-x)$Na_{0.5}Bi_{0.5}TiO_3$-x$KNbO_3$ (NBT-xKN), with x=0.02-0.08 were fabricated by solid state reaction and sintering. The crystal structures and dielectric properties were measured for different KN contents. All compositions in the unpoled, as-sintered state were found to be single phase pseudo-cubic. However, typical ferroelectric behaviour, with well-saturated polarisation-electric field hysteresis loops, was observed for certain compositions at high electric field levels. It is shown using high energy synchrotron XRD that the application of the electric field induced an irreversible structural transformation from the nano-polar pseudo-cubic phase to a ferroelectric rhombohedral phase. The changes in lattice elastic strain and crystallographic texture of a poled NBT-0.02KN specimen as a function of the grain orientation, ψ, conform well to those expected for a conventional rhombohedrally-distorted perovskite ferroelectric ceramic. The dielectric permittivity-temperature relationships for all compositions exhibit two transition temperatures and a frequency–dependent behaviour that is typical of a relaxor ferroelectric. The transition temperatures and grain size decrease with increasing KN content.

Key words: Lead-free, Piezoelectric ceramic, Domain switching, Phase transformation, Ferroelectric properties, Synchrotron x-ray diffraction.

1. Introduction

Lead-based piezoelectric ceramic materials have been used in many applications due to their superior electrical and electro-mechanical properties, especially lead zirconate titanate (PZT) which is a typical perovskite piezoceramic.[1] Materials having compositions close to the morphotropic phase boundary between tetragonal and rhombohedral phases have proved to show the best piezoelectric coefficients and coupling factors, which both play an essential role in actuators and sensors.[1] However, for the sake of protecting the environment, an increasing number of scientists have focused attention on lead-free piezoelectric ceramics in order to replace PZT. Among the various families of lead-free piezoelectric ceramics, $Na_{0.5}Bi_{0.5}TiO_3$ (NBT) is one of the most promising piezoelectric materials due to its high remanent polarisation at room temperature and relatively high Curie temperature.[2] To overcome its potential weaknesses such as high conductivity and large coercive field, many binary or ternary solid solutions have been investigated such as NBT-$SrTiO_3$,[3] NBT-$K_{0.5}Bi_{0.5}TiO_3$,[4] NBT-$BaTiO_3$,[5] NBT-$K_{0.5}Na_{0.5}NbO_3$,[6] NBT-$BaTiO_3$-$CaTiO_3$[7] and NBT-$BaTiO_3$-$K_{0.5}Na_{0.5}NbO_3$;[8] it is also supposed that the properties in these systems are improved as a result of forming morphotropic phase boundaries.

Another typical perovskite-type ferroelectric material, $KNbO_3$ (KN), is also a potential candidate for lead-free piezoelectrics due to its high Curie temperature and large remanent polarisation.[9] By forming a binary solid solution with $NaNbO_3$, compositions based on $K_{0.5}Na_{0.5}NbO_3$ have been identified as important lead-free solid solutions for piezoelectric applications.[10]

In the NBT-xKN system, a morphotropic phase boundary located at x=0.05 between pseudo-cubic and rhombohedral phases was reported by Fan.[11] However, a contradictory report of mixed rhombohedral and orthorhombic phases at x=0.05 was described by Pisitpipathsin.[12] Also, in a recent publication, it has been observed that such materials could possess useful electro-caloric properties.[13] Therefore, in this paper the structure, ferroelectric and dielectric properties of NBT-xKN have been investigated in order to clarify the remaining questions concerning its structure and functional properties.

2. Experimental methods

In this study, analytical-grade powders: Na_2CO_3(99.8%), K_2CO_3(99%), Bi_2O_3(99%), TiO_2(99%), Nb_2O_3(99%) were used as raw materials to prepare NBT-xKN (x=0.02,0.04,0.06,0.08) ceramics. The mixed powders were milled for 24 h in propan-2-ol using zirconia milling balls and then calcined for 10 h at 900 °C to accomplish the solid state reaction. The calcined powders were re-milled for 24 h to break down the particle agglomerates. The final dry powders were pressed into 6.5 mm diameter pellets under a uniaxial pressure of 150 MPa and sintered at 1180°C for 3 h in air.

The sintered ceramic samples, having a relative density of approximately 95%, were lightly ground, coated by silver paste (Gwent group) and fired at 500 °C for 30 min to form electrodes. The specimens for measurement of ferroelectric properties were poled in a silicone oil bath by applying six complete cycles of an electric field of 5.5 kV mm^{-1} at a frequency of 2 Hz. Ferroelectric polarisation-electric field (P-E) and current density-electric field (J-E) loops were obtained using the method described previously.[14] The dielectric properties of the as-fired (unpoled) samples were measured over a range of temperatures, from 50 to 400 °C, at frequencies of 1 kHz, 10 kHz and 100 kHz with a HP 4284A LCR meter, using a heating rate of 2 °C min^{-1}. For the purpose of phase pre-identification, all ceramic pellets were measured by laboratory based powder x-ray diffraction, using a Philips X'pert MPD Diffractometer at a wavelength of 1.542 Å. Specimens were ground on their major surfaces using 1200-grade SiC abrasive paper and thermally annealed at 500°C for 30 minutes to remove any residual strain induced during preparation. Additional XRD studies were performed at beamline I15 of the Diamond Light Source using high energy, monochromatic X-rays with a photon energy of 67 keV. The X-ray beam was focused down to 70 micron in diameter and cleaned up with the pinhole directly in front of the sample. 2-dimensional XRD images were recorded using a Perkin-Elmer XRD1621 flat-panel detector positioned approximately 1 m from the sample. These images were converted into conventional 1-dimensional XRD patterns corresponding to a range of grain orientations, ψ, relative to the poling direction, using Fit2D.[15] The profiles for selected diffraction peaks were fitted using X-fit.[16]

3. Results and discussion

The lab x-ray diffraction patterns obtained for NBT-xKN (x=0.02-0.08) ceramic pellets are illustrated in Fig. 1. All of the patterns are consistent with the presence of a single-phase perovskite structure with no evidence of phase coexistence. There is no obvious peak splitting, although some peak broadening was apparent, indicating that a predominantly pseudo-cubic phase was present for all compositions. Further high resolution diffraction studies are required to identify any subtle distortions from the cubic structure. According to Fan,[11] a {111} peak doublet was observed for unpoled ceramics having compositions NBT-0.02KN and NBT-0.04KN; this type of peak splitting was not found in the present results. Also, unlike Pisitpipathsin's report,[12] there was no evidence for an MPB between rhombohedral and orthorhombic phases at x=0.05.

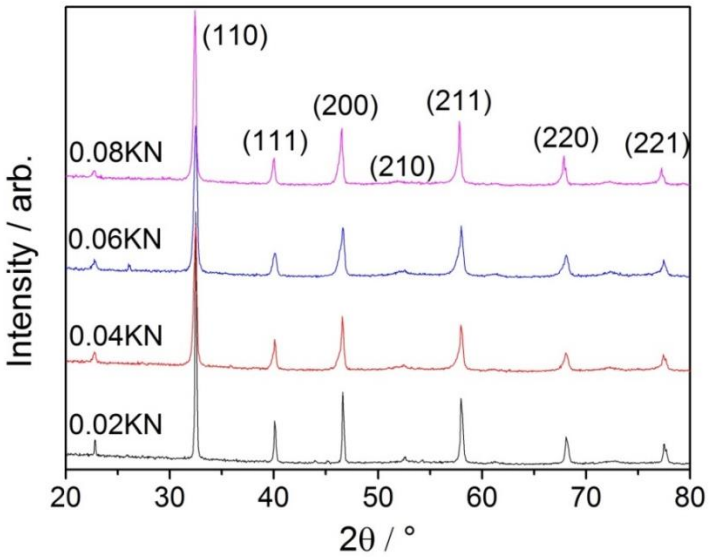

Fig. 1. X-ray diffraction patterns for all compositions of NBT-xKN as-sintered ceramics.

The microstructures of the NBT-0.02KN and NBT-0.08KN ceramics are presented in Fig. 2. NBT-0.02KN (Fig. 2(a)) exhibited an irregular morphology and a grain size of approximately 5.1 μm. However, NBT-0.08KN (Fig. 2(b)) showed a cuboidal grain shape with a reduction in the average grain size to approximately 2.3 μm. Therefore, it is apparent that increasing the KN content leads to a decrease in grain size and enhanced uniformity in microstructure.

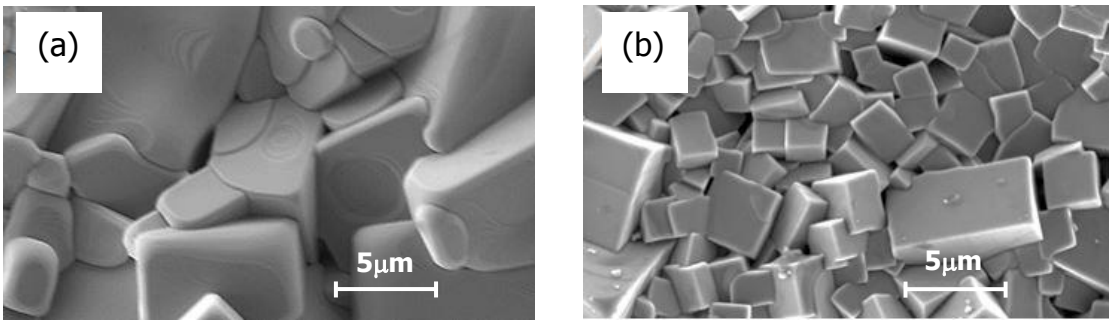

Fig. 2. SEM images of fracture surface of ceramic pellets sintered at 1180 °C for 3 h (a) NBT-0.02KN and (b) NBT-0.08KN.

The P-E and J-E loops of NBT-xKN ceramics measured at room temperature under an AC electric field of 5.5 kV mm^{-1} are presented in Fig 3. NBT-0.02KN exhibits a saturated P-E loop with a remanent polarisation, P_r, of 0.23 C m^{-2} and a single switching peak in the J-E curve, indicating its typical ferroelectric behaviour.[7] A slight constriction in the middle of the P-E loop and a splitting of the current switching peak were observed in both NBT-0.04KN and NBT-0.06KN, indicating an electric field-induced weak-polar to ordered ferroelectric phase transformation.[7] The two peaks in the J-E curve correspond to the forward electric field, E_f , associated with the weak-polar to ordered ferroelectric phase transformation, and the backward electric field, E_b, associated with the reverse transformation respectively.[7] A slim P-E loop with nearly zero remanent polarisation was found for NBT-0.08KN, which suggests that the electric field-induced transformation to the ordered ferroelectric phase did not occur for this composition.

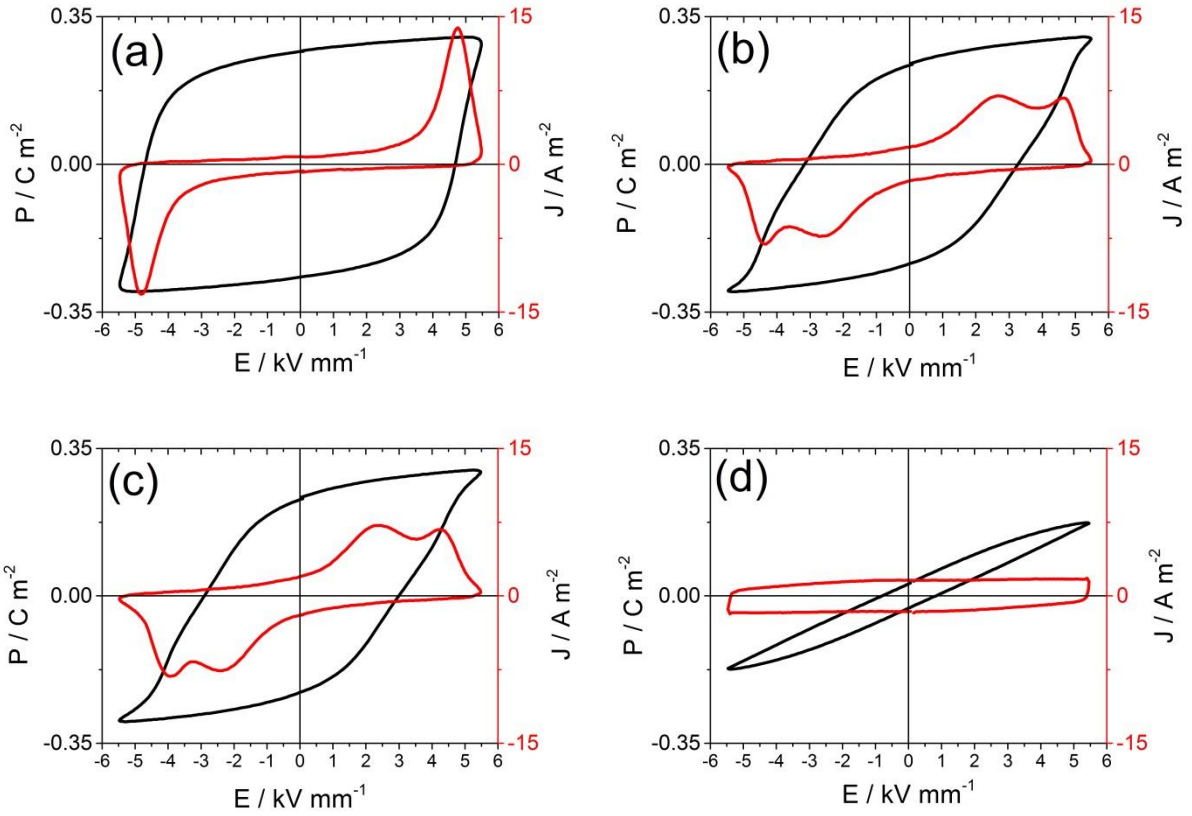

Fig. 3. P-E and J-E curves of NBT-xKN sintered ceramics measured at 5.5 kV mm^{-1} and 2 Hz (a) NBT-0.02KN, (b) NBT-0.04KN, (c) NBT-0.06KN, and (d) NBT-0.08KN.

The temperature-dependence of dielectric permittivity and loss tangent of NBT-xKN as-sintered ceramic pellets are shown in Fig. 4. In the lower temperature region, all dielectric permittivity curves exhibit a frequency-dependence, which is characteristic of relaxor ferroelectrics. To be more specific, aliovalent Na^+, Bi^{3+} and K^+ share the A-site while Ti^{4+} and Nb^{5+} share the B-site in the ABO_3 perovskite structure. Increasing site disorder due to K^+ and Nb^{5+} ions enhances the relaxor ferroelectric behaviour in the lower temperature range.[17] Two anomalies in the dielectric curve represent the high-temperature dielectric peak, T_{max}, and the lower-temperature structural

transformation temperature, T_c. Both of these temperatures decrease with increasing KN content, which is consistent with the previous publications.[11, 17] According to Fan, [11] the low-temperature peak in the dielectric permittivity-temperature curve was said to be associated with the thermal depolarisation temperature. This point has not yet been proven and requires further investigation.

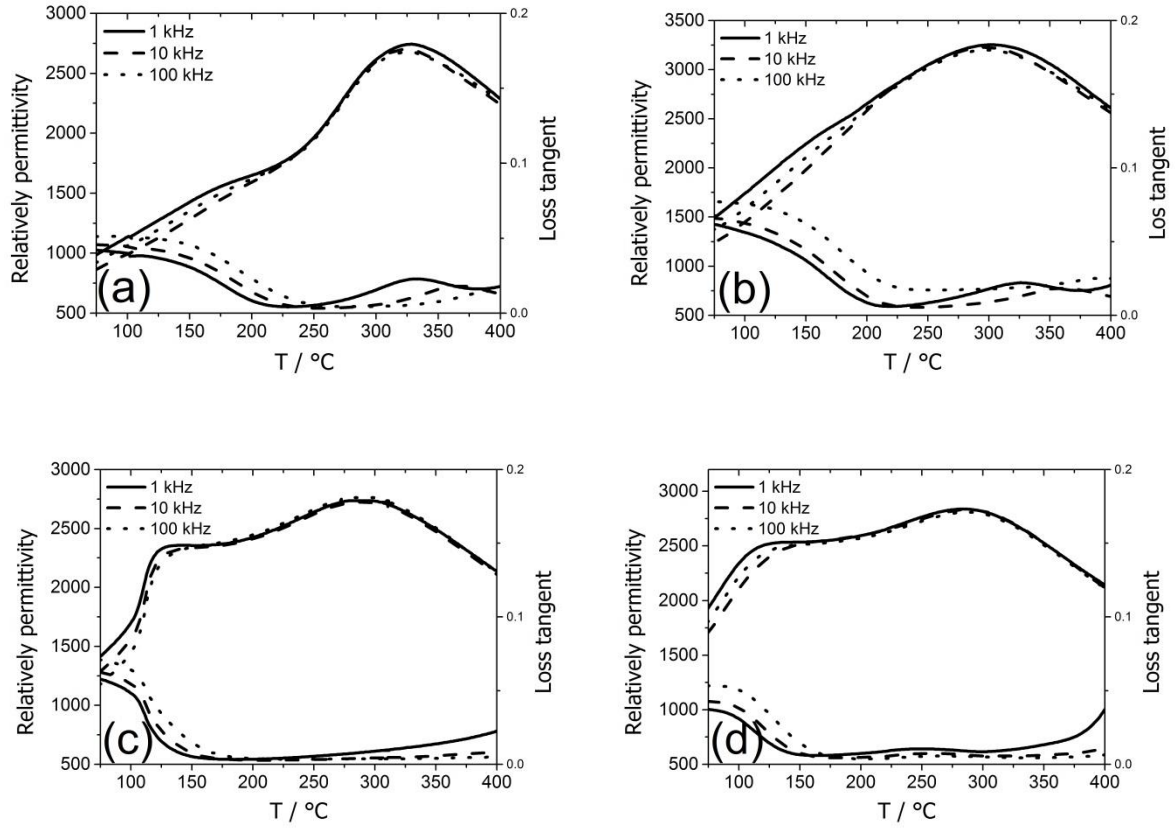

Fig. 4. Temperature dependence of dielectric permittivity and loss for unpoled NBT-xKN unpoled ceramic pellets (a) x=0.02, (b) x=0.04, (c) x=0.06 and (d) x=0.08, measured at frequencies of 1, 10 and 100 kHz.

As noted above, the x-ray diffraction patterns for all of the as-sintered ceramics appeared to indicate the presence of a pseudo-cubic phase, with no obvious peak splitting. However, certain compositions, such as NBT-0.02KN, showed well-developed ferroelectric hysteresis loops with a relatively high remanent polarisation (Fig. 2(a)). A similar phenomenon was reported by Daniels,[18] who observed an electric field-induced structural transformation from pseudo-cubic to tetragonal in NBT-0.07$BaTiO_3$ ceramics; the tetragonal phase also exhibited orientation-dependent ferroelectric domain switching behaviour.[18]

In order to evaluate the influence of the electric field on the structure of NBT-xKN ceramics, the XRD patterns of unpoled and poled specimens were measured using high-energy synchrotron XRD on beamline I15 at the Diamond light source. Selected area diffraction patterns for a range of different grain orientations are illustrated in Fig. 5. The splitting of the {111} peak after poling at 5.5 kV mm^{-1} confirms the

presence of the rhombohedral phase. The variations in the relative intensities of the {111} peaks as a function of the azimuthal angle ψ indicates that the [111]-oriented domains are oriented preferentially along the electric field direction at ψ = 0°. Furthermore, for the poled specimen the {200} peak exhibits a slight shift as function of ψ, indicating an elastic lattice strain. These observations are similar to those made previously for poled rhombohedral PZT ceramics.[19]

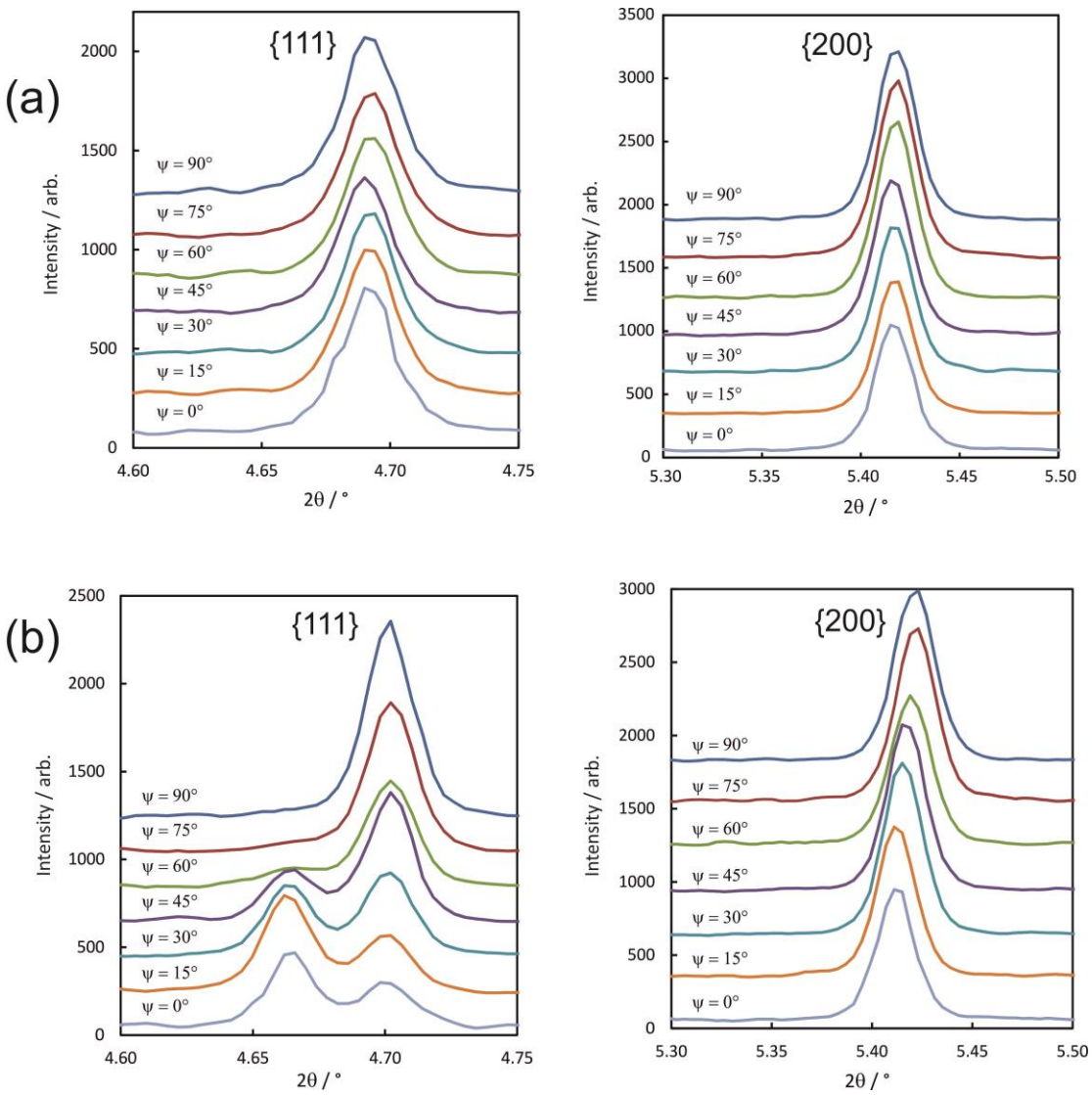

Fig. 5. {111} and {200} diffraction peak profiles for (a) unpoled and (b) poled NBT-0.02KN ceramics as a function of the grain orientation, ψ.

First, consider the origin of the lattice strain, which is most clearly evident for the {200} peak. In polycrystalline ferroelectric ceramics, the process of poling leads to domain reorientation with an associated macroscopic strain. After removal of the applied electric field, the piezoelectric strain reduces to zero but a tensile remanent strain, $\bar{\varepsilon}$, remains along the poling direction, ψ = 0°. Assuming a volume conservative domain switching mechanism and transverse isotropy of the material, the transverse strain

(ψ = 90°) is $-\bar{\varepsilon}/2$. Therefore, the macroscopic strain due to poling can be represented in the co-ordinate system *X* of the specimen as [20]

$$\varepsilon^{P}(X) = \begin{pmatrix} -\bar{\varepsilon}/2 & 0 & 0 \\ 0 & -\bar{\varepsilon}/2 & 0 \\ 0 & 0 & \bar{\varepsilon} \end{pmatrix} \quad (1)$$

The X_3 axis is chosen as the direction of the applied electric field, which corresponds to ψ = 0°. In the modified co-ordinate system, *Y*, in which the axis Y_3 is rotated by an angle ψ relative to the axis X_3, the elongation along Y_3 is given by [20]

$$\varepsilon_{33}^{P}(Y) = \bar{\varepsilon}\left(\frac{3}{2}\cos^2\psi - \frac{1}{2}\right) \quad (2)$$

In rhombohedrally-distorted perovskite ferroelectrics, the <h00> orientation of a grain has the special property that its dimension is independent of the fractions of different domain variants present within the grain and consequently it would remain unchanged after poling in an unconstrained state. This point was explained more thoroughly in a previous publication.[20] However, each grain in a polycrystalline ceramic is constrained by its neighbours. Therefore, after the removal of the electric field and the associated piezoelectric strain, the observed lattice strain for a {200}-oriented grain is due solely to the macroscopic strain of its surroundings and the local inter-granular residual stresses.[20] For this reason, it is anticipated that the {200} lattice spacing, d_{200} and the lattice strain, ε_{200}, should both exhibit a dependence on grain orientation, ψ, that is similar in form to equation 2 (neglecting the influences of crystalline anisotropy and initial residual stresses).[21]

Determination of the lattice strain demands knowledge of the unstrained lattice parameter, d^0_{200}, which is usually obtained from diffraction measurements on an unpoled specimen. Unfortunately, it was not possible to use this approach in the present case due to the nature of the poling process for the NBT-0.02KN ceramics, which involved both a cubic to rhombohedral phase transformation and ferroelectric domain reorientation in the rhombohedral phase. Also, it was found that attempts to create a random domain structure by thermal depolarisation caused a reversion to the cubic phase, as will be reported in a subsequent publication. As an alternative approach, it is possible to estimate the value of d^0_{200} by utilizing the relationship given in equation 2 above, since it is evident that the macroscopic elongation due to poling is zero when $\cos^2\psi = 1/3$, or ψ = 54.7°.

The positions of the {200} diffraction peaks were determined by peak profile fitting using *X-fit* and the lattice spacing, $d_{\{200\}}$, calculated using the Bragg equation. Plotting $d_{\{200\}}$ as a function of $\cos^2\psi$ yielded a linear relationship, as illustrated in Fig. 6(a). By fitting these data using a least-squares method, it was determined that the value of d^0_{200} was approximately equal to 0.19455 nm. The change in lattice strain, ε_{200}, as a

function of ψ was subsequently calculated using this value of d^0_{200}; the results of these calculations are illustrated in Fig. 6(b). It is apparent that the dependence of ε_{200} on ψ exhibited a good fit to equation (2), although it should also be noted that the lattice strain is not exactly equal to the macroscopic strain due to the effects of elastic anisotropy and the Poisson effect.[22]

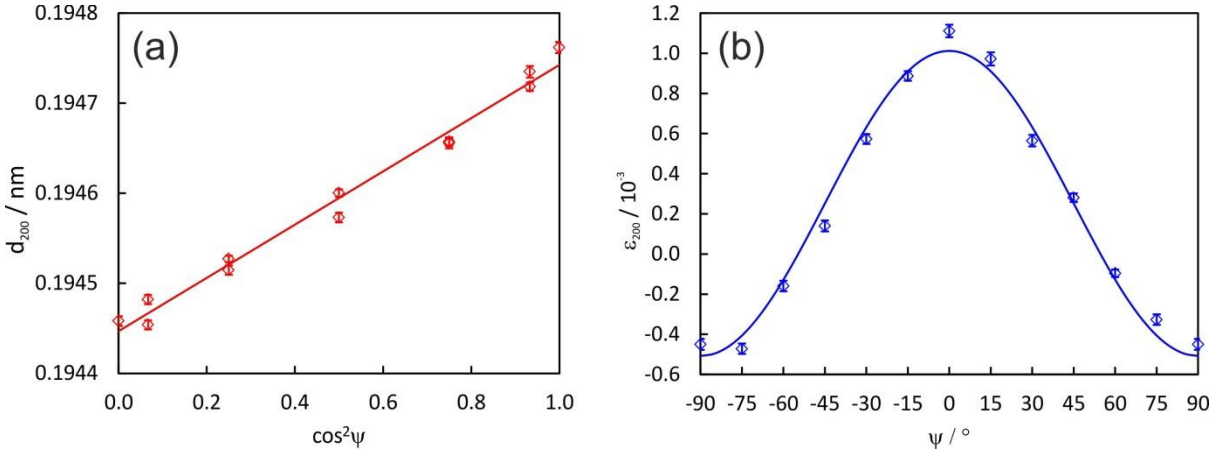

Fig. 6. Dependence of (a) d_{200} and (b) ε_{200} on azimuthal angle, ψ. Symbols are experimental data points and solid lines are calculated according to equation (2).

Next, consider the change in the differently-oriented domain variants as a function of grain orientation. The simplest method to calculate the volume fraction of [111]-oriented domains, v_{111}, involves using the ratio of the integrated intensities of the {111} diffraction peaks.[19]

$$R_1(111) = \frac{I_{111}}{I_{111} + I_{\bar{1}\bar{1}\bar{1}}} \tag{3}$$

Note that $I_{\bar{1}\bar{1}\bar{1}}$ includes contributions from the $(\bar{1}\bar{1}\bar{1})$, $(1\bar{1}\bar{1})$ and $(11\bar{1})$ reflections.

It was found that the ratio, R_1, exhibited an approximately linear dependence on $\cos^2\psi$, as shown in Fig. 7(a). For reasons similar to those given above, it is anticipated that the value of R_1 should be equal to that of an unpoled specimen, having random domain orientations, when $\cos^2\psi = 1/3$. However, the linear fit to the data shown in Fig. 7(a) indicated that the intensity ratio was approximately equal to 0.219 at $\cos^2\psi = 1/3$, which is significantly smaller than the value of 0.25 expected for random domain texture. This apparent discrepancy can be understood as being due to slight differences in the structure factors for the (111) and $(\bar{1}11)$ diffraction peaks.

The fractions of differently-oriented domains can be calculated more accurately by adapting the method described by Jones for tetragonally-distorted perovskite ferroelectrics to the rhombohedral case.[23] According to this approach, the fraction of [111]-oriented domains in a rhombohedral specimen is given by

$$\nu_{111} = \frac{I_{111}/I'_{111}}{I_{111}/I'_{111} + 3I_{\bar{1}11}/I'_{\bar{1}11}} \tag{4}$$

where I'_{hkl} represents the intensity of the (hkl) reflection for the unpoled, randomly oriented specimen. Equation (4) can also be expressed in terms of the simple peak intensity ratio $R_2(111)$, defined as

$$R_2(111) = \frac{I_{111}}{I_{\bar{1}11}} \tag{5}$$

Substituting equation (5) into (4) leads to the following expression for the [111] domain volume fraction, ν_{111}.

$$\nu_{111} = \frac{R_2}{R_2 + 3R'_2} \tag{6}$$

The value of the peak intensity ratio in the unpoled state, R_2', can be found from R_1' since R_2 and R_1 are generally related according to

$$R_2 = \frac{R_1}{(1 - R_1)} \tag{7}$$

The value of R_1' was determined as approximately 0.219, as discussed above, which yields a value of 0.281 for R_2'.

The variations in ν_{111}, calculated from the measured diffraction peak intensities according to equations (5) and (6), are presented in Fig. 7(b). These results indicate that the degree of non-180° domain switching in the remanent state was relatively high, with a maximum ν_{111} value of approximately 0.7 being achieved for ψ = 0°. This level of saturation is very similar to that of the *soft* rhombohedral PZT ceramic reported by Hall.[19] Also, it is clearly evident that the domain orientation distribution function follows closely the form of the macroscopic strain, according to equation (2). Therefore, we can conclude that the electric field-induced metastable rhombohedral phase of the NBT-0.02KN ceramic exhibits both structural and functional characteristics that are typical of a conventional long-range ordered ferroelectric.

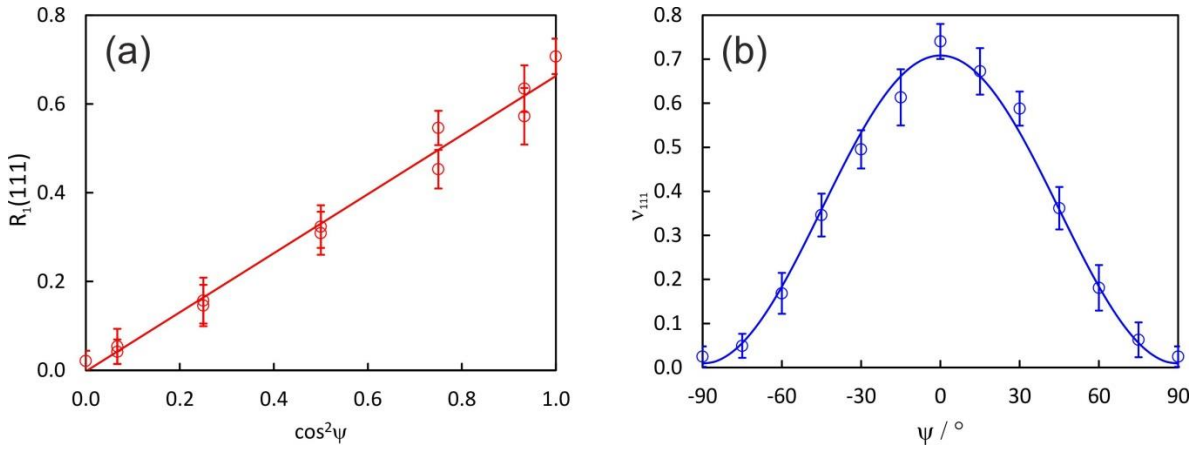

Fig. 7. Dependence of (a) peak intensity ratio, $R_1(111)$, and (b) domain fraction, ν_{111}, on azimuthal angle, ψ. Symbols are experimental data points and solid lines are calculated using a squared cosine relation.

4. Conclusions

The results of XRD analysis indicated that all of the as-sintered NBT-xKN ceramics appeared to be pseudo-cubic, which is a typical characteristic of relaxor ferroelectrics. On the other hand, ferroelectric hysteresis measurements suggested that either reversible (for x = 0.04 and 0.06) or irreversible (for x = 0.02) transformations to a conventional ferroelectric phase could occur under the influence of a high electric field. The irreversible transformation to a metastable rhombohedral ferroelectric phase for NBT-0.02KN was confirmed by analysis of the diffraction patterns for a poled specimen, using high-energy synchrotron XRD. The transition temperatures, T_m and T_c, obtained from temperature-dependent dielectric measurements, and the grain size observed using SEM, were all found to decrease with increasing KN content.

5. Acknowledgements

The authors are grateful for support provided by Diamond Light Source Ltd under experiment number EE8699.

6. References

1. J. Rödel, W. Jo, K. T. P. Seifert, E.-M. Anton, T. Granzow, and D. Damjanovic, *J. Am. Ceram. Soc.*, 2009, **92**(6), 1153-1177.
2. G. A. Smolenskii, V. A. Isupov, A. I. Agranovskaya, and N. N. Krainik, *Sov. Phys. Solid State*, 1961, **2**(196), 2651.
3. K. Sakata and M. Yoichiro, *Ferroelectrics*, 1974, **7**(1), 347-349.
4. Y. Hiruma, H. Nagata, and T. Takenaka, *J. Appl. Phys.*, 2008, **104**(12).
5. W. Jo, S. Schaab, E. Sapper, L. A. Schmitt, H.-J. Kleebe, A. J. Bell, and J. Rödel, *J. Appl. Phys.*, 2011, **110**(7), 074106.
6. A. B. Kounga, S.-T. Zhang, W. Jo, T. Granzow, and J. Rödel, *Appl. Phys. Lett.*, 2008, **92**(22).
7. G. Viola, R. McKinnon, V. Koval, A. Adomkevicius, S. Dunn, and H. Yan, *J. Phys. Chem. C*, 2014, **118**(16), 8564-8570.
8. J. E. Daniels, W. Jo, J. Rödel, V. Honkimäki, and J. L. Jones, *Acta Mater.*, 2010, **58**(6), 2103-2111.
9. G. Shirane, H. Danner, A. Pavlovic, and R. Pepinsky, *Phys. Rev. Lett.*, 1954, **93**, 672-673.
10. Y. Saito, H. Takao, T. Tani, T. Nonoyama, K. Takatori, T. Homma, T. Nagaya, and M. Nakamura, *Nature*, 2004, **432**(7013), 84-87.
11. G. Fan, W. Lu, X. Wang, and F. Liang, *Appl. Phys. Lett.*, 2007, **91**(20).
12. N. Pistipipathsin, W. Koontasing, S. Eitssayeam, U. Intatha, G. Rujijanagul, K. Pengpat, and T. Tunkasiri, *Adv. Mater. Res*, 2008, **55-57**, 225-228.
13. X. Jiang, L. Luo, B. Wang, W. Li, and H. Chen, *Ceram. Int.*, 2014, **40**, 2627-2634.
14. D. A. Hall, P. J. Stevenson, and T. R. Mullins, *Brit. Cer. Proc.*, 1997, **57**, 197-211.
15. A. P. Hammersley, S. O. Svensson, M. Hanfland, A. N. Fitch, and D. Hausermann, *High Pressure Res.*, 1996, **14**(235).
16. A. A. Coelho and R. W. Cheary, *CCP14 Library* http://www.ccp14.ac.uk, 1996.
17. X. Jiang, B. Wang, L. Luo, W. Li, J. Zhou, and H. Chen, *J. Solid State Chem.*, 2014, **213**(0), 72-78.
18. J. E. Daniels, W. Jo, J. Rödel, and J. L. Jones, *Appl. Phys. Lett.*, 2009, **95**(3).
19. D. A. Hall, A. Steuwer, B. Cherdhirunkorn, T. Mori, and P. J. Withers, *J. Appl. Phys.*, 2004, **96**(8), 4245-4252.
20. D. A. Hall, A. Steuwer, B. Cherdhirunkorn, T. Mori, and P. J. Withers, *Acta Mater.*, 2006, **54**(11), 3075-3083.
21. L. Daniel, D. A. Hall, J. Koruza, K. G. Webber, A. King, and P. J. Withers, *J. Appl. Phys.*, 2015, **117**(17), 174104.
22. D. A. Hall, A. Steuwer, B. Cherdhirunkorn, P. J. Withers, and T. Mori, *J. Mech. Phys. Solids*, 2005, **53**(2), 249-260.
23. J. L. Jones, E. B. Slamovich, and K. J. Bowman, *J. Appl. Phys.*, 2005, **97**(3), 034113.